 doi.org/10.52568/001430/JCSP/46.02.2024

Development Metronidazole Nanocomposite as Anti-inflammatory Agent for Athletes using Full Factorial Design

[1]Hazem Abdul Kader Sabbagh, [1,2]Samer Hasan Hussein-Al-Ali*, [3]Zead Abudayeh, [3]Rami Ayoub
[3]Qais Ibrahim Abdallah Abualassa and [4]Nashwan Abdallah Nashwan
[1]*Department of Basic Pharmaceutical Sciences, Faculty of Pharmacy, Isra University, Amman 11622, Jordan*
[2]*Department of Chemistry, Faculty of Science, Isra University, Amman 11622, Jordan.*
[3]*Department of Applied Pharmaceutical Sciences and Clinical Pharmacy, Faculty of Pharmacy, Isra University, Amman 11622, Jordan.*
[4]*Faculty of Arts, Isra University, Amman 11622, Jordan.*
samer.alali@iu.edu.jo*

(Received on 30th January 2023, accepted in revised form 24th August 2023)

Summary: This work considers the optimization and characterization of metronidazole-calcium alginate nanoparticles (MET-AlgNPs) by an ionotropic gelation technique. The effect of the amount of sodium alginate (Alg), metronidazole, and calcium chloride ($CaCl_2$) as the factors affecting drug loading efficiency (LE), particle size and potential of formulations were optimized and analyzed by using multiple regressions. These formulations were characterized by X-ray diffraction (XRD), Fourier transform infrared spectroscopy (FTIR), Thermogravimetric analysis (TGA), zeta size and potential, scanning electron microscope (SEM) and in vitro drug release studies. XRD, FTIR, and TGA analysis indicated the presence of drug in MET-AlgNPs nanocomposites. In vitro drug released from nanocomposites was carried out and showed that the release rate of MET from the MET-AlgNPs nanocomposites was very slow. These results indicate an extended release of the drug from its respective nanocomposites, and therefore these nanocomposites have good potential to be used as extended-release formulations of the drug.

Keywords: Metronidazole, Multiple regression analysis, Nanocomposites, Sodium alginate**.**

Introduction

Metronidazole (MET) is a nitroimidazole antibiotic primarily introduced in the 1950s [1]. It is effective against anaerobic bacteria; Gram-negative anaerobes such as *Bacteroides* spp, *Fusobacterium* spp, *Porphyromonas* spp, and *Prevotella* spp. In addition, MET is quite effective against Gram-positive anaerobes such as *Peptostreptococci*, and *Clostridia* spp [2, 3]. Metronidazole enters the bacterial cell by passive diffusion. The cytotoxic effect is produced from nitroso free radicals which are produced by the transference of an electron from various donors to the nitro group. This drug interacts with intracellular proteins, DNA or RNA, leading to the inhibition of repair and disrupted transcription which consequently lead to cell death [4, 5]. It is still used so far because of its strong activity, low cost, and good pharmacodynamic and pharmacokinetic properties. MET is available in oral, intravenous, and topical forms and has excellent bioavailability. However, this antibiotic has many side effects such as dry mouth, nausea, vomiting, anorexia, and mineral taste [6, 7]. As recommended by the British National Formulary, it can be taken in a dose of 200 mg each 8 hours for 3–7 days. Scientists studied the absorption of MET for in dosage forms, such as tablets, topical, and suppositories and found that the oral absorption was 100% depending on calculations that used equivalent intravenous doses as a reference. The rectal absorption was 67 – 82% of the intravenous parameters. The topical absorption was low, and the intravaginal bioavailability was 56% when compared with a 500 mg intravenous dose [8-13].

Entamoeba histolytica uses proteases to contravene intestinal mucosa or to enter the portal circulation, creating hepatic abscess and then killing host cells [14]. The treatment is with metronidazole or tinidazole followed by iodoquinol or paromomycin [15, 16]. The pole treatment of Traveler's diarrhea is fluid replacement. Antibiotic therapy should be taken for athletes that develop moderate to severe diarrhea, which is recommended by the International Society of Travel Medicine as distressing and interfering with planned activities; fever; or blood, pus, or mucus in the stool. If a parasitic cause is suspected, metronidazole 500 mg 3 times daily for 5 days is the preferred regimen [17].

Researchers have recently been working on nanotechnology, especially in drug delivery fields, to reduce unwanted side effects of drugs [18]. Polymeric nanoparticles have been important in recent years due to their use in drug delivery as

*To whom all correspondence should be addressed.

carriers [19-21]. In the pharmaceutical industry, neutral polymers can be used as drug delivery systems, such as alginate and chitosan [22, 23]. This can be attributed to their good availability, low cost, biocompatibility, degradability, and nontoxicity [24].

Novel therapies using nanocarriers and their conjugates with metronidazole can provide an excellent solution for drug enhancement. For example, silver nanoparticles- polyethylene glycol-metronidazole (AgNPs-PEG-MET) was used to treat Periodontal disease [25-27]. Chitosan nanoparticles-metronidazole was used to against *Giardia* infection in hamsters [28-30]. Gold nanoparticles-metronidazole capped was used in against *Helicobacter pylori* [31]. Zinc oxide nanoparticles-metronidazole was used against *Staphylococcus aureus* bacterial strains [32]. Montmorillonite nanodevices for the colon metronidazole delivery [33]. Polyethyleneimine-metronidazole was used for treatment of *Staphylococcal* Skin Infections [34].

Thus, optimization of the physicochemical properties of the prepared formulations such as loading efficiency, size, and surface charge are considered a challenge for preparing these formulations.

Multiple regressions are presented to learn more about the correlation between several independent or predictor variables and a dependent or criterion variable. In pharmaceutical science and drug formulation, multiple regression procedures are widely used [35, 36].

The goal of the current work is to study the statistical relationship between a response variable (LE, size, and potential) and explanatory variables (Alg, drug and $CaCl_2$ concentrations). An option to know the relationship is to employ regression analysis.

Experimental

Materials

The chemicals which were used in this study are metronidazole ($C_6H_9N_3O_3$ (99% purity), Sigma-Aldrich) and, low viscosity sodium alginate (10-100 kDa), AZ chem., Sigma Aldrich). High Performance Liquid Chromatography (HPLC) grade acetonitrile (99.8%, FW 41.05) was purchased from VWR International, LLC - West Chester, PA. All other chemicals including acetic acid, calcium chloride, sodium phosphate dibasic, sodium phosphate monohydrate, and sodium chloride were purchased from Chem CO (England).

Preparation of alginate nanoparticles and MET-AlgNPs nanocomposites

Alginate nanoparticles (AlgNPs) were prepared by ionic gelation method according to the literature [37]. In brief, cross-linking agents of calcium chloride ($CaCl_2$) solutions with masses 50, 75, and 100 mg were added to different masses of sodium alginate (100, 200, 400 mg) dropwise at the flow rate of 0.1 ml/s. At the same time, the pH was controlled at 5.2. The solution was continuous stirring at room temperature for 18 hours. Subsequently, the suspension was centrifuged at 10000 rpm for 15 min and the supernatant was discarded and washed with deionized water and dried in an oven at 40°C. The same procedure was repeated for the formation of MET-AlgNPs nanocomposites using different masses of metronidazole (100, 200, and 400 mg).

Physico-chemical analysis and characterization

Powder X-ray Diffraction

The crystal phase identification of the prepared nanoparticles and nanocomposites samples was carried out using X-ray diffraction (XRD). It is an advanced technique which is widely used for the characterization of crystalline materials. The XRD technique was recorded in the range of 2–70° on a Shimadzu diffractometer, XRD-6000.

Infrared spectroscopy

FTIR is a technique used for the identification of functional groups and chemical bonds that are present in a molecule, interpreted from the observed infrared absorption spectrum. This technique can be used as supporting data, which complements other techniques to indicate that intercalation instead of adsorption has occurred.

For this purpose, Fourier transform infrared (FTIR) spectra of the materials were recorded over the range of 400–4000 cm^{-1} on a Perkin Elmer (model Smart UAIR-two) with 4 cm^{-1} resolutions.

The metronidazole loading efficiency.

The ultra-centrifugation instrument was used to determine the loading efficiency (LE) of MET from the prepared nanocomposites. The procedure was as follows: 2.0 ml of suspension was centrifuged (Hettich Universal 30 RF) at 10000 rpm for 10 min in

an ultra-filtration centrifuge. Finally, the free drug was measured by high performance liquid chromatography (HPLC, Shimadzu, Japan). The UV detection wavelength was 323 nm. Venusil C18 column (4.6 mm × 250 mm, 5 μm) was used to analyze the samples. The column temperature was kept at 25 °C. The mobile phase consisted of a mixture of acetonitrile/0.1% phosphoric acid (5:95, v/v) and the flow rate was 1.0 ml/min. The LE were calculated as follows:

$$\%\,\text{Loading Effciency (LE)} = \frac{T_p - T_f}{\text{mass of nanopartic les}} \times 100 \quad (2)$$

where T_p is the total MET used to prepare the nanoparticles, and T_f is the free MET in the supernatant.

Controlled release study of metronidazole from the respective nanocomposites

In-vitro release of MET from nanocomposites were determined using a Perkin Elmer UV-Vis spectrophotometer with λ_{max} of 323 nm. A suitable amount of each nanocomposite was added to 2 mL of the media. The cumulative amount of drug released into the solution was measured at preset time intervals at the corresponding λ_{max}.

The percentage release of the MET into the release media was obtained by:

$$\%\,\text{Release} = \frac{\text{Concentrat ion of MET at time t (ppm)}}{\text{Concentrat ion correspond ing to 100\% release of MET (ppm)}} \times 100$$

3

The concentration which corresponds to 100% release was obtained by adding an identified amount of nanocomposites in 2 mL PBS by using sonicate and heat the nanocomposites at 37 ^{o}C

Model optimization and validation.

Detection of multicollinearity in Regression Analysis

Multicollinearity occurs when independent variables in a regression model are correlated. This correlation will effect on the fit of the model. One method to evaluate multicollinearity is the variance inflation factor (VIF), which assesses how much the variance of an estimated regression coefficient increases if your predictors are correlated. If no factors are correlated, the VIFs will all be 1.

Based on the absence of multicollinearity in the readings in this work, as shown in Table-1, the data will be analyzed statistically using multivariate regression model.

Multiple regressions are an extension of the simple linear regression. It is used when we want to predict the value of a variable based on the value of two or more other variables. The variable we want to predict is called the dependent variable (or sometimes, the outcome, target, or criterion variable). The variables we are using to predict the value of the dependent variable are called the independent variables (or sometimes, predictor, explanatory, regressor variables or response).

Checking the validity of the assumptions for LE, Potential and size models

To check the validity of the model and the assumption that all the error terms are identically and independently normally distributed with mean zero; we used different methods explained in the following section. The others method will keep as supplementary data.

Pareto chart of response standardized effect

A bar graphic, known as Pareto chart, was used as a graphical representation for evaluating the effects of the main factors and their interactions on the response sorted by their absolute size. Fig 1 shows the bars of the main factors (A=Alg, B=$CaCl_2$, and C=MET) and their combinations arranged in descending order

The vertical line is the statistical threshold for a level of significance ($P<0.05$). The bars which cross that line show that the main factors or their combinations have statistical significance on the response.

From the results presented in Fig 1A, it can be clearly seen that two main factors (Alg, and MET) and $CaCl_2$*$CaCl_2$, Alg*Alg, and Alg*$CaCl_2$ have a statistically significant effect on the LE.

Fig 1C shows that different factors affect the potential response. It can be clearly seen that all main factors (Alg, $CaCl_2$, and MET), Square factors ($CaCl_2$*$CaCl_2$) and 2- way interaction (Alg*$CaCl_2$ and, Alg*MET) have a statistically significant effect on the response. In the case of size in Fig 1D, a descending order according to their effect estimates that they are: Alg, MET*MET, and $CaCl_2$.

Table-1: Analysis of Variance (ANOVA) for loading efficiency (LE%), particle size, and zeta potential.

	loading efficiency (LE%)				particle size				zeta potential			
Source	**F Value**	**P Value**	**T Value**	**VIF**	**F Value**	**P Value**	**T Value**	**VIF**	**F Value**	**P Value**	**T Value**	**VIF**
Model	89.2	0.000	8.81	-	11.4	0.000	9.1	-	11.7	0.000	-12.1	-
Alg	433.9	0.000	20.8	1.15	88.7	0.000	9.4	1.07	7.8	0.015	-2.8	1.16
$CaCl_2$	0.7	0.430	0.82	1.11	5.7	0.032	2.4	1.08	26.6	0.000	5.2	1.18
MET	106.2	0.000	10.3	1.11	0.2	0.647	0.5	1.11	36.0	0.000	-6.0	1.25
Alg*Alg	23.2	0.000	4.8	1.13	2.1	0.170	-1.4	1.04	3.4	0.089	1.8	1.14
$CaCl_2$*$CaCl_2$	43.5	0.000	6.6	1.16	0.1	0.801	-0.3	1.05	25.5	0.000	-5.1	1.09
MET*MET	2.7	0.127	-1.6	1.07	3.2	0.097	-1.8	1.12	0.3	0.633	0.5	1.09
Alg*$CaCl_2$	1.0	0.343	1.0	1.28	0.4	0.541	0.6	1.06	25.6	0.000	5.1	1.15
Alg*MET	13.2	0.003	3.6	1.36	2.0	0.184	1.4	1.06	21.1	0.001	-4.6	1.21
$CaCl_2$*MET	1.64	0.224	1.3	1.36	2.2	0.157	1.5	1.01	0.2	0.696	0.4	1.14
R^2	**R^2 = 98.5, R^2 (adj) = 97.4**				**R^2 = 88.0, R^2 (adj) =80.3**				**R^2 = 89.0, R^2 (adj) = 81.4%**			
Regression equation	**LE= 135.6 - 0.1621 Alg - 3.465 $CaCl_2$ + 0.0572 MET + 0.000476 Alg*Alg + 0.02181 $CaCl_2$*$CaCl_2$ – 0.000157 MET*MET + 0.000387 Alg*$CaCl_2$ + 0.000250 Alg*MET + 0.000538 $CaCl_2$*MET**				**Size= -114 + 1.214 Alg + 0.55 CaCl2 + 0.451 MET - 0.00160 Alg*Alg - 0.0094 CaCl2*CaCl2 - 0.00218 MET*MET + 0.00271 Alg*CaCl2 + 0.000950 Alg*MET + 0.00585 CaCl2*MET**				**Potential=-36.42 - 0.0719 Alg + 0.841 $CaCl_2$- 0.0054 MET +0.000076 Alg*Alg - 0.00625 CaCl2*$CaCl_2$ + 0.000018 MET*MET +0.000698 Alg*$CaCl_2$ - 0.000106 Alg*MET + 0.000057 $CaCl_2$*MET**			

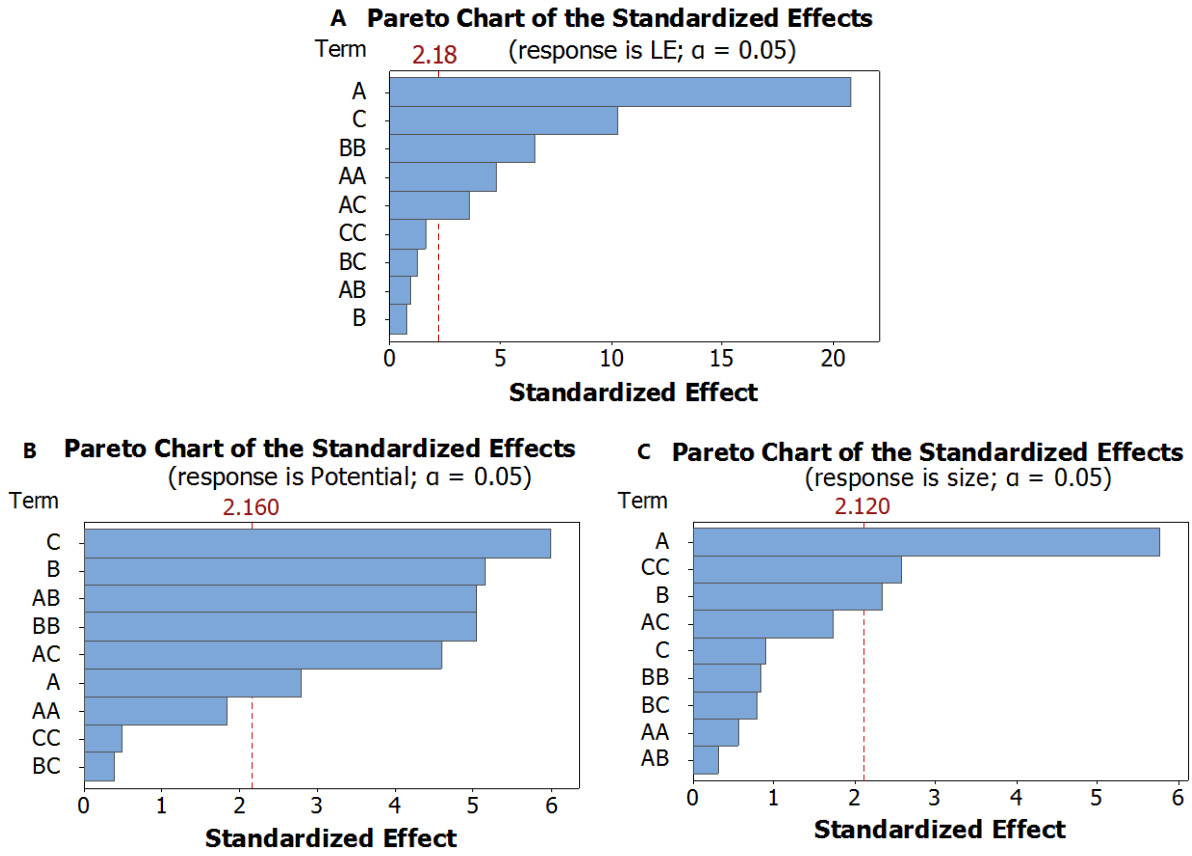

Fig. 1: Pareto charts of different standardized effects for LE (A), zeta potential (B), particle size (C).

Contour plot and surface plot of LE, zeta potential and particle size with selected independent variables.

To know about the effect of variables on the responses, the researcher used three-dimensional surface plots (3D) and contour plots (2D).

Effect of Alg, MET, and $CaCl_2$ concentrations on LE.

From Figs 2A and B, the MET concentrations have a significant effect on the LE. This increase in the loading with the increase of alginate concentration can be attributed to increasing of alginate concentration which leads to forming a dense network structure with cohesive vacancies (pores) that entrap the essential oils droplets (proper pores size with homogeneous distribution).

The effect of $CaCl_2$ concentration on the LE at the highest concentration of MET is shown in Fig 2C. The results showed a direct proportion between them, this may be explained by the increase in the alginate cross-linking and compactness of the formed insoluble nanocomposites. These results are in agreement with Takka and Mirghani researchers [38, 39]. On the other hand, Ostberg et al. reported that less drug was encapsulated at higher calcium concentration [40]. It was also found that further increase in the concentration of $CaCl_2$ did not enhance the drug loading. This could be due to the possible saturation of calcium binding sites in the guluronic acid chain, preventing further calcium ion entrapment and, hence, cross-linking was not altered with higher concentrations of calcium chloride solution.

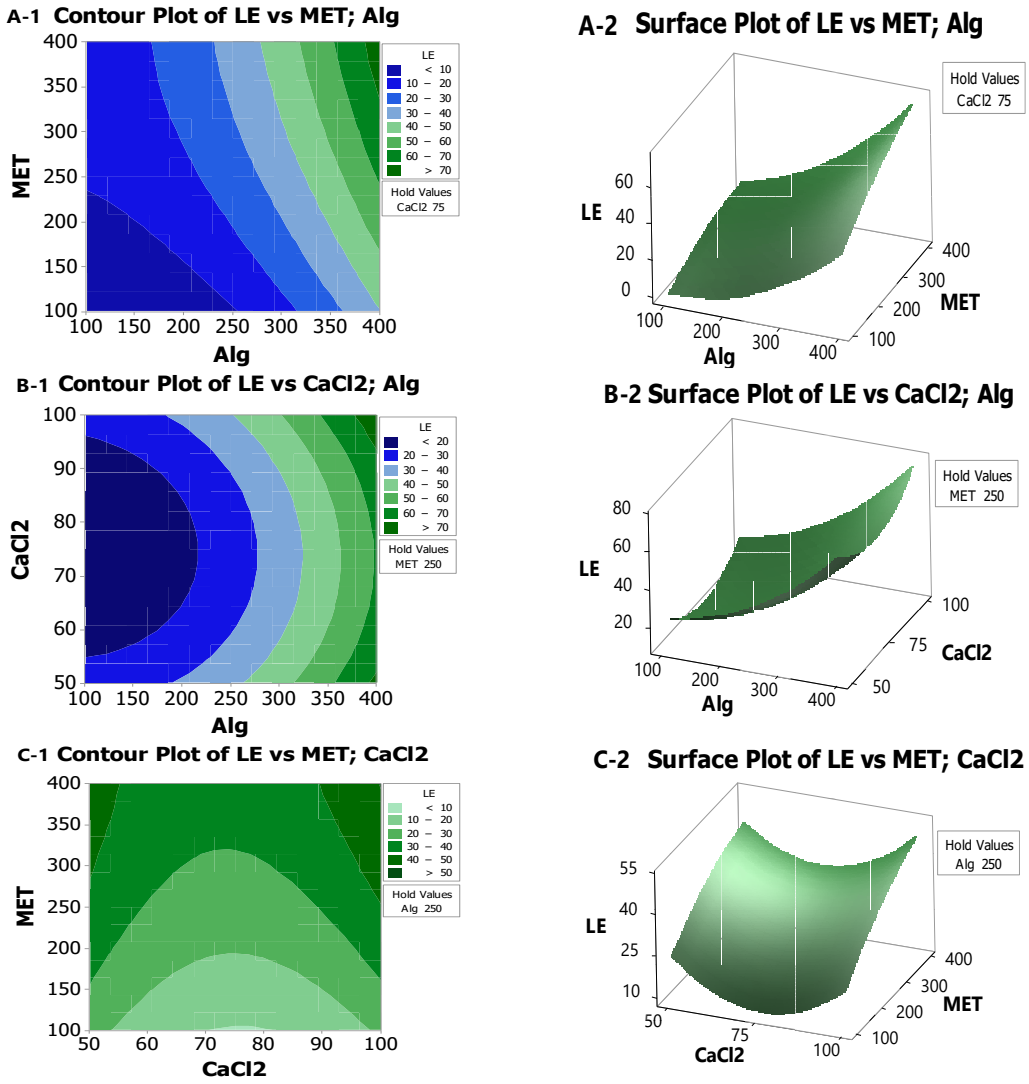

Fig. 2: The contour plot and response surface of the LE with variances of $CaCl_2$, MET, and Alg concentrations.

Effect of Alg, MET, and CaCl2 concentrations on particle size.

The model has a high F-value of 11.4, which implies that the model is significant ($p<0.000$), Table 1. In this case, Alg, $CaCl_2$, and MET*MET are significant model terms. The model terms are not significant if the values are greater than 0.1000. If many insignificant model terms are present in the model, model reduction is required to improve the model. In the present case, it is required as most of them are more than 0.100, which indicates that the particle size is predominantly affected by factors Alg, $CaCl_2$, and MET*MET and the influence of other factors are negligible.

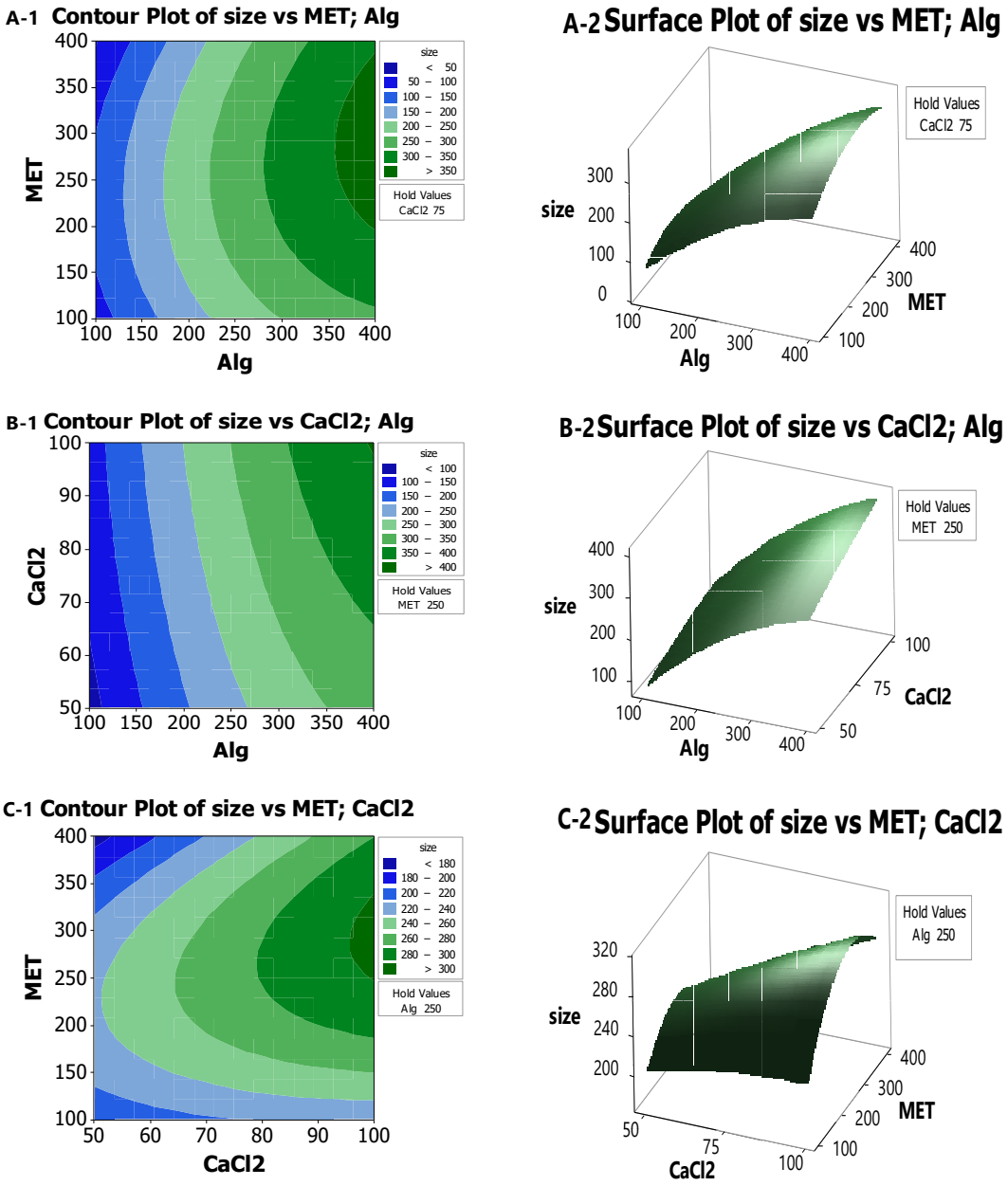

Fig. 3: The contour plot and response surface of the size with variances of $CaCl_2$, MET, and Alg concentrations.

In the above regression equation (Table 2), Alg and $CaCl_2$ represent the main effects on size. MET*MET are interactive terms which stand for the nonlinear relationship between the responses. The positive sign in the equation represents synergistic effect and the negative sign denotes antagonistic effect on the particle size. This equation states that the two variables Alg and $CaCl_2$ have a positive effect on the particle size, whereas the MET*MET concentration has a negative effect over particle size. From the equation and Fig 3, it is apparent that as the Alg was increased from 100 to 400 mg, the particle size increased correspondingly. Increasing the concentration of the polymer in the preparation increases the frequency of collisions between the particles during preparation. These results in the fusion of semi-formed particles produce a collective increase in particle size.

From Figs 3B and C, increasing the concentration of $CaCl_2$ in the preparation means that there is an increase in the particle size. It has been reported in our work that concentrations of alginate have effects on the particle size. As can be seen from Table 1 and Fig 3, MET-AlgNPs nanocomposites ranging from 19.7±1.4 to 421.8±25 nm was achieved. The increase in the concentration of alginate in the preparation increased the particle size of the nanocomposites. This is because the increase of alginate concentration leads to more functional groups coming together around the calcium crosslinking agent and therefore more layers of alginate chains were able to join the calcium cations [41].

Effect of Alg, MET and CaCl2 concentrations on zeta potential.

The model F value of 11.7 implies that the model is significant. In this model, Alg, $CaCl_2$, MET, $CaCl_2$*$CaCl_2$, Alg* MET, and Alg* $CaCl_2$ are significant model terms as the Prob > F values are below 0.05, as mentioned earlier. The R^2 value of 89.0 % is close to the Adj R^2 value of 81.4% as expected.

The equation in Table 1 shows that the Alg and MET concentrations have a negative impact on zeta potential, whereas $CaCl_2$ concentration has a positive impact as shown in Fig 4. Zeta potential is a measurable parameter which provides information on the electrostatic potential of particles in solution and depicts their formulation stability. Although some high potentials (> +30 mV or < -30 mV) is considered favorable for better stability of formulation dispersion, a near neutral zeta potential is preferred for particles intended for systemic administration. Neutral or low negative charge is often preferred to avoid interference by plasma components in vivo. A positive zeta potential frequently causes toxicity due to intrinsic binding affinity towards cellular components [42]. In this study, NPs showed negative zeta potential <-22 mV and > -12 mV; this is because the COOH groups on the backbone of the alginate are deprotonated [43].

There was a feeble dependence of charge upon the concentrations of Alg, $CaCl_2$, and MET; and their interactive effect $CaCl_2$*$CaCl_2$, Alg*$CaCl_2$, and Alg*MET. An increase in the Alg concentration in Fig 4A tends to decrease the negativity of the zeta potential at low concentration of MET and increase the negativity of the zeta potential at high concentration of MET. From Fig 4B, the potential of -22 mV is given by high concentration of Alg and low concentration of $CaCl_2$. A similar observation was collected (-22 mV) by using high concentration of MET and low concentration of $CaCl_2$ (Fig 4C).

Optimization and validation

From the selected mathematical model. The optimized % LE was 78.2%. In addition, the minimizing particle size was 263.4 nm and −12.8mV zeta potential.

The comparison of experimental results with predicted values is shown in Table 2. From the table, the theoretical values for the response were close to the experimentally obtained values. This result indicates that the mathematical model can be successfully used to predict the %LE, particle size and zeta potential values for any combination of Alg, MET, and $CaCl_2$within the range of the performed experimentation.

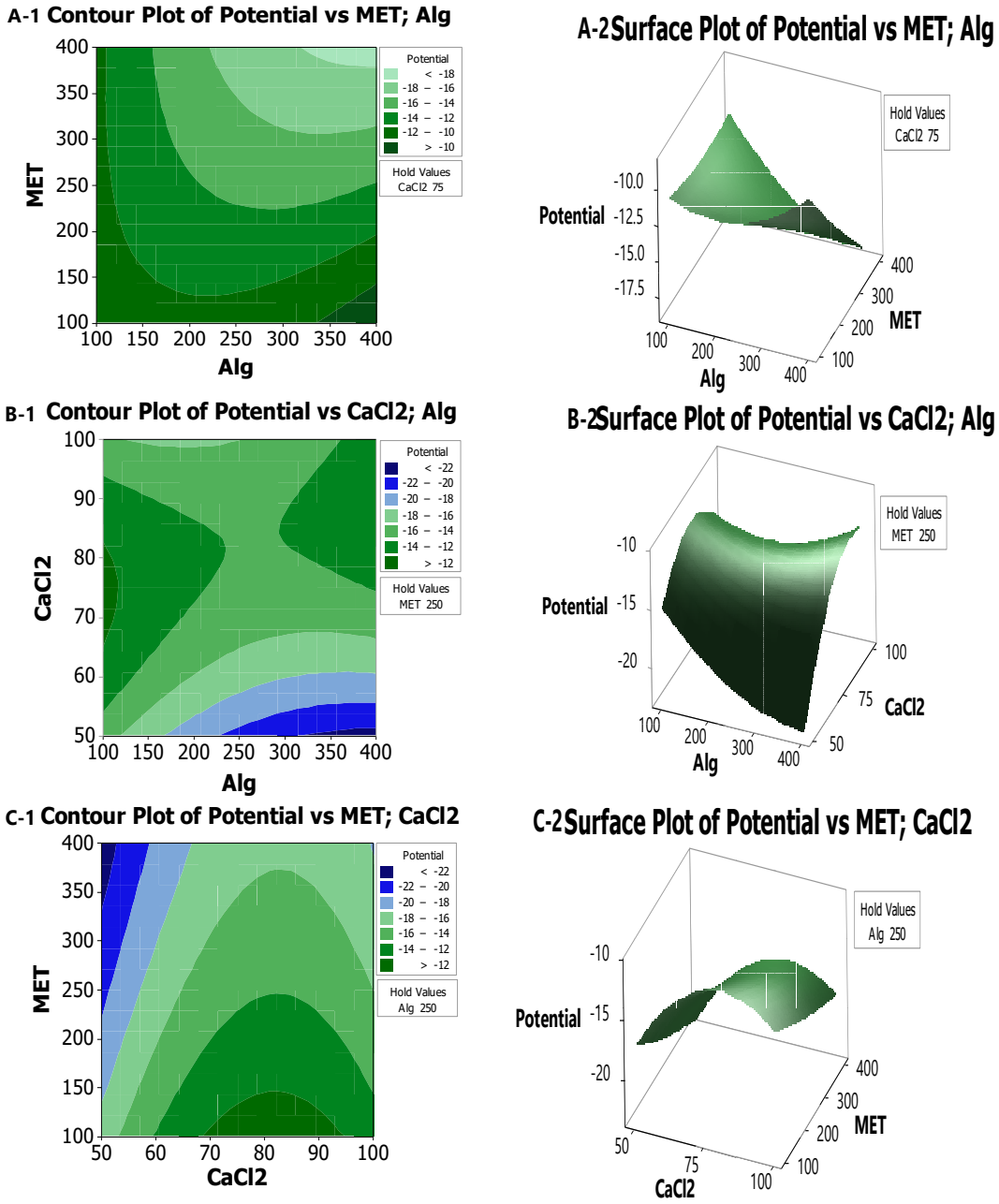

Fig. 4: The contour plot and response surface of the potential variances of $CaCl_2$, MET, and Alg concentrations.

Table-2: Response optimization for LE, particle size, and zeta potential.

No.	Alg	MET	$CaCl_2$	%LE			Particle Size (nm)			Zeta Potential (mV)		
				Exp	Theo	Error %	Exp	Theo	Error %	Exp	Theo	Error %
1	309	244	98	54	58	6.9	471	455	3.5	-14.8	-12.8	15.6
2	362	196	71	46	50	8.0	353	369	4.3	-11.4	-10.3	10.7
3	204	277	84	29	35	17.1	289	295	2.0	-12.8	-10.8	18.5

Characterization of the optimized formulation

X-ray diffraction (XRD) for MET-CSNPs nanocomposite

Fig 5 represents the XRD patterns of MET, AlgNPs, and MET-AlgNPs. In Fig 5A, the pattern of MET revealed sharp crystalline peaks at 13.5 ° and 24.9 °. These data suggested that MET was in a crystalline state. In Fig 5B ,three diffraction peaks at 2θ values 14.1º, 21.8º, and 39.1º were observed for AlgNPs due to the reflection of their (110) plane from the polyguluronate unit, (200) plane from polymannuronate and the other from amorphous halo [44, 45]. In the case of MET-AlgNPs in Fig 5C, the sharp peaks for MET were not found in the pattern of the MET-AlgNPs, indicating that MET was molecularly dispersed in the polymers [46].

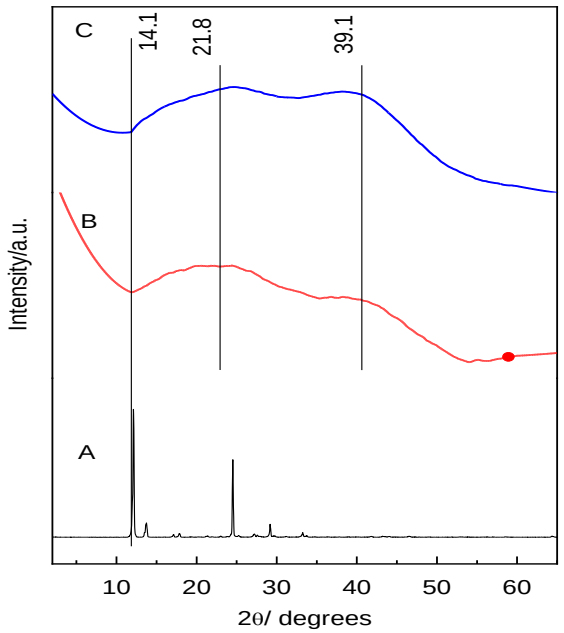

Fig. 5: XRD diffraction spectra of MET (A), AlgNPs (B), and MET-AlgNPs nanocomposites (C).

FTIR spectroscopic analysis of AlgNPs and MET-AlgNPs

The FTIR spectra of the Alginate, AlgNPs, and MET-AlgNPs were recorded and compared (Fig 6). Spectrum of Alginate (Fig 6A) shows different absorption bands regarding hydroxyl, ether, and carboxylic functional groups. Stretching vibrations of O–H bonds appeared at 3278 cm^{-1}. Stretching vibrations of aliphatic C–H were observed at 2892 cm^{-1}. The bands at 1594 and 1408 cm^{-1} were attributed to asymmetric and symmetric stretching vibrations of COO^- ion, respectively [41]. The bands at 1100 and 946 cm^{-1} were attributed to the C–O stretching vibration of the pyranosyl ring. On the other hand, The FTIR spectra of AlgNP in Fig 12B exhibited characteristic bands at 1591 cm^{-1} and 1417 cm^{-1} indicating the involvement of COO- group in the coordination process with Ca^{++}; and 3266 cm^{-1} due to the hydroxyl group with Ca^{++} [47]. Absorption band of O–H bonds in AlgNPs appeared narrower than Alginate. This difference is due to the sharing of O-H and COO^- groups of alginate to the Ca^{++} to form a chelating structure and the consequent decrease in hydrogen bonding between hydroxyl functional groups which affords a narrower band in AlgNPs. In the FTIR spectrum of MET-AlgNPs in Fig 12D the spectra of MET-AlgNPs have similarity to the spectra of AlgNPs, and some peaks were not shifted in wave numbers significantly indicating only occurrence of electrostatic interaction between MET with alginate.

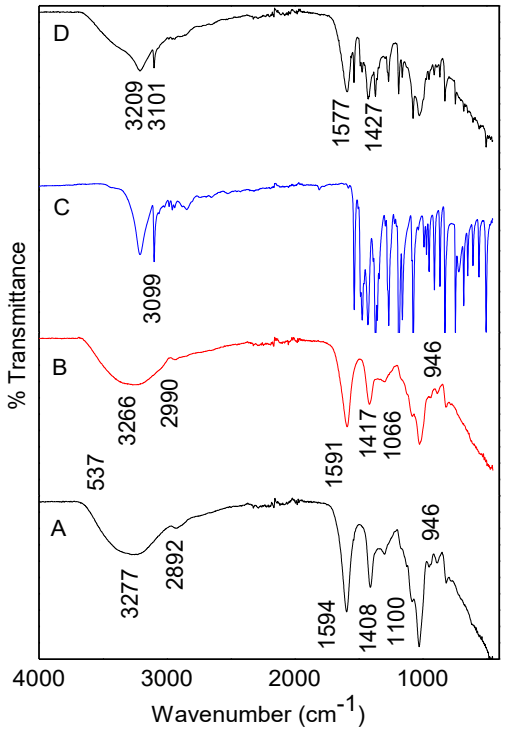

Fig. 6: FTIR spectra of n-Alg (A), AlgNPs (B), MET (C), and MET-AlgNPs (D).

Thermogravimetric analysis (TGA) of MET-AlgNPs nanocomposites

Fig 7 illustrates the TGA curve of pure MET, AlgNPs, and MET-AlgNPs. TGA of AlgNPs

shows the decomposition between 27-184 ºC which is due to the loss of water molecules trapped in the samples. The principal weight loss occurred between 238 ºC to 397 ºC with a maximum 26.3% weight loss, corresponding to the decomposition of its alginate backbone structure. Incorporation of MET in the alginate matrix increases the polymer decomposition temperature and weight loss. There are numerous reports which state that incorporation of drug materials in the polymer matrix usually increases the thermal stability of the polymer as well as weight loss [48].

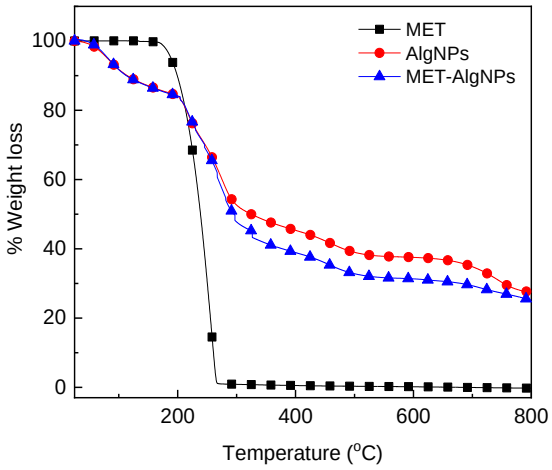

Fig. 7: TGA curves are shown for free MET, AlgNPs, and MET-AlgNPs nanocomposites.

Release properties of MET from MET-AlgNPs nanocomposites

The MET release results from MET-AlgNPs nanocomposites have a burst effect in the first hour release. By looking closely at the sample during the first hour, it was found that the optimized samples gave the release at 27% (Fig 8). On the other hand, the MET release from the sample was completed after 24 hours.

The release of MET from MET-AlgNPs can be explained by the fact that the sodium salt of alginate consists of guluronic and mannuronic acid units, which is transformed to gel in the presence of Ca^{2+} ions during formation AlgNPs. This leads to the formation of an insoluble calcium alginate complex [49]. From our results in Fig 8, the study shows the extended release properties of the formulations ,similar to the literature [50, 51].

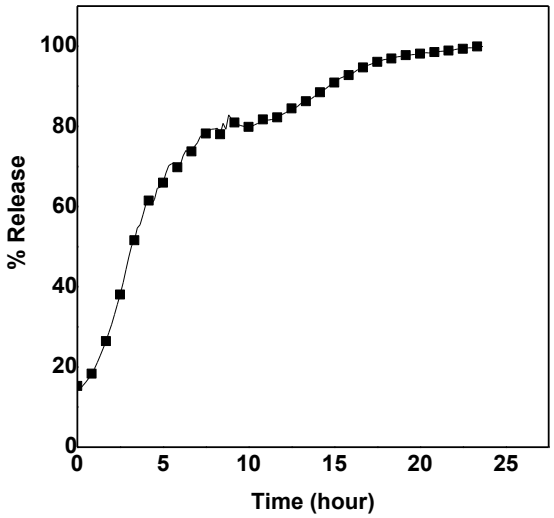

Fig. 8: *In-vitro* release behaviours of MET from MET-AlgNPs nanocomposites in the 0.1N HCl.

Release kinetics of drug from the MET-AlgNPs nanocomposite

The data of the cumulative release of the MET from nanocomposites were fitted to five kinetic models which generally are described as follows:

1. The linear form of first-order kinetic model as Equation (4)
$$\ln (q_e - q_t) = \ln q_e - k_1 t \quad (4)$$

where q_e and q_t are the quantity released at equilibrium and the quantity released at any time (t), respectively, and k_1 is the rate constant of the pseudo-first-order release kinetics.

2. The linear form of second-order kinetic equation may be represented in Equation (5)
$$t/q_t = 1/k_2 q_e^2 + t/q_e \quad (5)$$

where, k_2 is the rate constant of the pseudo-second-order release kinetics.

3. The Higuchi model describes the increased release of the drug from the nanocomposites with increasing square root of time.

$$q_t = K_H \sqrt{t} \quad (6)$$

where k_H is the Higuchi rate constant.

4. The Hixson-Crowell model gives the relationship between the cube root of the

percentage of drug remaining in the nanocomposites as a function of time.

$$\sqrt[3]{M_o} - \sqrt[3]{q_t} = Kt \quad (7)$$

where M_o is the initial amount of drug in the nanocomposites and q_t is the quantity released at time t.

5. The Korsmeyer-Peppas model gives the relationship between the log of the percentage of drugs released and the log of time

$$\frac{q_t}{q_\infty} = Kt^n \quad (8)$$

where q_∞ is the release at infinite time.

The MET release from nanocomposites was discussed by first-order kinetics, second-order kinetics, Hixson-Crowell model, and Korsmeyer-Peppas model. The data shows the nanocomposite follows Korsmeyer- Peppas model with R^2 value 0.823, comparing to first-order kinetics, second-order kinetics, and Hixson-Crowell models which shows R^2 value 0.805, 0.672 and 0.735, respectively.

Conclusion

One of the principal objectives of the research work was to control the release of nanocomposites and drug delivery systems using metronidazole and sodium alginate. In the research work, increased Alg level in the formulations resulted in increased LE and size. The effect of drug concentrations was much more significant statistically on the LE, but it has no effect on the size. In-vitro drug release from nanocomposites was carried out using the first, second, Hixson-Crowell, and Korsmeyer-Peppas models and showed that the release followed the Korsmeyer- Peppas. The rate of MET from the MET-AlgNPs nanocomposites was very slow. These results indicate an extended release of the drug from its respective nanocomposites, and therefore these nanocomposites have good potential to be used as extended-release formulations of the drug.

Declaration of conflicting interests

The authors report no conflicts of interest in this work.

Acknowledgement

The author would like to thank the Faculty of Pharmacy at Isra University for providing funding for this research. This study was also supported by Hikma Pharmaceuticals Research and Development Department.

References

1. D. Videau, Action of a metronidazole-spiramycin association on anaerobic bacteria, *Pathol Biol*, **19**, 661 (1971).
2. C. D. Freeman, N. E. Klutman and K. C. Lamp, Metronidazole, *Drugs*, **54**, 679 (1997).
3. Y. Roche and R. N. Yoshimori, In-vitro activity of spiramycin and metronidazole alone or in combination against clinical isolates from odontogenic abscesses, *J. Antimicrob. Chemother*, **40**, 353 (1997).
4. S. I. Doron, K. R. Beaulac, A. Dhand and D. R. Snydman, in *Antimicrobial Drug Resistance*, Springer, 281 (2017).
5. M. Müller, Mode of action of metronidazole on anaerobic bacteria and protozoa, *Surgery*, **93**, 165 (1983).
6. C. Dollery, Testing and control of therapeutic materials and drugs, *Acta Odontol. Venez.*, **11**, 28 (1973).
7. K. C. Lamp, C. D. Freeman, N. E. Klutman and M. K. Lacy, Pharmacokinetics and pharmacodynamics of the nitroimidazole antimicrobials, *Clin. Pharmacokinet*, **36**, 353 (1999).
8. G. Houghton, P. Thorne, J. Smith, R. Templeton, P. Cook and I. James, (1979).
9. H. Mattie, B. Dijkmans and C. Van Gulpen, The pharmacokinetics of metronidazole and tinidazole in patients with mixed aerobic—anaerobic infections, *J. Antimicrob. Chemother*, **10**, 59 (1982).
10. J. Mattila, P. Männistö, R. Mäntylä, S. Nykänen and U. Lamminsivu, Comparative pharmacokinetics of metronidazole and tinidazole as influenced by administration route, *Antimicrob Agents Chemother*, **23**, 721 (1983).
11. I. K. Aronson, J. A. Rumsfield, D. P. West, J. Alexander, J. H. Fischer and F. P. Paloucek, Evaluation of topical metronidazole gel in acne rosacea, *Ann. Pharmacother*, **21**, 346 (1987).
12. L. Schmadel and G. McEvoy, Topical metronidazole: a new therapy for rosacea, *Clin. Pharm*, **9**, 94 (1990).
13. F. E. Cunningham, D. M. Kraus, L. Brubaker and J. H. Fischer, Pharmacokinetics of

intravaginal metronidazole gel, *J. Clin. Pharmacol*, **34**, 1060 (1994).
14. S. L. Stanley, Amoebiasis, *The lancet*, **361**, 1025 (2003).
15. L. W. Kitchen, Case studies in international travelers, *Am. Fam. Physician*, **60**, 471 (1999).
16. C. C. Young, M. W. Niedfeldt, L. M. Gottschlich, C. S. Peterson and M. R. Gammons, Infectious disease and the extreme sport athlete, *Clin. Sports Med.*, **26**, 473 (2007).
17. C. A. Jaworski and V. Rygiel, Acute illness in the athlete, *Clin. Sports Med*, **38**, 577 (2019).
18. S. Bhatia, *Natural Polymer Drug Delivery Systems: Nanoparticles, Plants, and Algae*, Springer, (2016).
19. Y. Hu, X. Jiang, Y. Ding, H. Ge, Y. Yuan and C. Yang, Synthesis and characterization of chitosan–poly (acrylic acid) nanoparticles, *Biomater.*, **23**, 3193 (2002).
20. E. D. Pressly, R. Rossin, A. Hagooly, K.-i. Fukukawa, B. W. Messmore, M. J. Welch, K. L. Wooley, M. S. Lamm, R. A. Hule and D. J. Pochan, Structural effects on the biodistribution and positron emission tomography (PET) imaging of well-defined 64Cu-labeled nanoparticles comprised of amphiphilic block graft copolymers, *Biomacromolecules*, **8**, 3126 (2007).
21. B. Sarmento, D. Ferreira, L. Jorgensen and M. Van De Weert, Probing insulin's secondary structure after entrapment into alginate/chitosan nanoparticles, *Eur J Pharm Biopharm*, **65**, 10 (2007).
22. Z. Dong, Q. Wang and Y. Du, Alginate/gelatin blend films and their properties for drug controlled release, *J. Membr. Sci*, **280**, 37 (2006).
23. S. Khamhan, Y. Baimark, S. Chaichanadee, P. Phinyocheep and S. Kittipoom, Water vapor permeability and mechanical properties of biodegradable chitosan/methoxy poly (ethylene glycol)-b-poly (ε-caprolactone) nanocomposite films, *Int J Polym Anal Ch*, **13**, 224 (2008).
24. M. Zohuriaan and F. Shokrolahi, Thermal studies on natural and modified gums, *Polym. Test.*, **23**, 575 (2004).
25. K. P. Steckiewicz, P. Cieciórski, E. Barcińska, M. Jaśkiewicz, M. Narajczyk, M. Bauer, W. Kamysz, E. Megiel and I. Inkielewicz-Stepniak, Silver nanoparticles as chlorhexidine and metronidazole drug delivery platforms: their potential use in treating periodontitis, *Int J Nanomedicine*, 495 (2022).
26. T. C. Jackson, A. A. Agboke, E. J. Udofa, A. S. Ucheokoro, B. E. Udo and N. L. Ifekpolugo, Characterization and release kinetics of metronidazole loaded silver nanoparticles prepared from Carica papaya leaf extract, *Adv in Nanopart.*, **8**, 47 (2019).
27. T. C. Jackson, B. O. Patani, N. L. Ifekpolugo, E. M. Udofa and N. M. Obiakor, Developent of metronidazole loaded silver nanoparticles from Acalypha ciliata for treatment of susceptible pathogens, *Nanosci. Nanotechnol.*, **9**, 22 (2019).
28. A. M. L. El-Gendy, M. A. A. Mohammed, M. M. I. Ghallab, M. O. A. Aziz and S. M. Ibrahim, Therapeutic effect of chitosan nanoparticles and metronidazole in treatment of experimentally giardiasis infected hamsters, *Iran. J. Parasitol.*, **16**, 32 (2021).
29. A. Oliveira, A. Araújo, L. C. Rodrigues, C. S. Silva, R. L. Reis, N. M. Neves, P. Leão and A. Martins, Metronidazole delivery nanosystem able to reduce the pathogenicity of bacteria in colorectal infection, *Biomacromolecules*, **23**, 2415 (2022).
30. H. A. K. Sabbagh, S. H. Hussein-Al-Ali, M. Z. Hussein, Z. Abudayeh, R. Ayoub and S. M. Abudoleh, A statistical study on the development of metronidazole-chitosan-alginate nanocomposite formulation using the full factorial design, *Polymers*, **12**, 772 (2020).
31. R. Fateh, A. Javadi, J. Kardan-Yamch, H. A. Rahdar, M. Amini, F. Ghasemi, A. Azimi, M. Davarpanah and R. Mohammadzadeh, Construction of metronidazole capped in gold nanoparticles against Helicobacter pylori: antimicrobial activity improvement, *Folia Med.*, **63**, 197 (2021).
32. S. A. Habeeb, A. H. Hammadi, D. Abed and L. F. Al-Jibouri, Green synthesis of metronidazole or clindamycin-loaded hexagonal zinc oxide nanoparticles from Ziziphus extracts and its antibacterial activity, *Pharmacia*, **69**, 855 (2022).
33. I. Calabrese, G. Cavallaro, C. Scialabba, M. Licciardi, M. Merli, L. Sciascia and M. L. T. Liveri, Montmorillonite nanodevices for the colon metronidazole delivery, *Int. J. Pharm*, **457**, 224 (2013).
34. F. D. Victorelli, G. M. F. Calixto, M. A. D. S. Ramos, T. M. Bauab and M. Chorilli, Metronidazole-loaded polyethyleneimine and chitosan-based liquid crystalline system for treatment of staphylococcal skin infections, *"J. Biomed. Nanotechnol.*, **14**, 227 (2018).
35. A. Kumar and K. K. Sawant, Application of multiple regression analysis in optimization of anastrozole-loaded PLGA nanoparticles, *J. Microencapsul.*, **31**, 105 (2014).

36. G. A. Fridgeirsdottir, R. J. Harris, I. L. Dryden, P. M. Fischer and C. J. Roberts, Multiple Linear Regression Modeling To Predict the Stability of Polymer–Drug Solid Dispersions: Comparison of the Effects of Polymers and Manufacturing Methods on Solid Dispersion Stability, *Mol. Pharmaceutics*, **15**, 1826 (2018).
37. N. Morsi, D. Ghorab, H. Refai and H. Teba, Preparation and evaluation of alginate/chitosan nanodispersions for ocular delivery, *Int. J. Pharm. Pharm. Sci*., **7**, 234 (2015).
38. S. Takka, Ö. H. Ocak and F. Acartürk, Formulation and investigation of nicardipine HCl–alginate gel beads with factorial design-based studies, *Eur. j. pharm. sci.*, **6**, 241 (1998).
39. A. Mirghani, N. M. Idkaidek, M. t. S. Salem and N. M. Najib, Formulation and release behavior of diclofenac sodium in Compritol 888 matrix beads encapsulated in alginate, *Drug Dev. Ind. Pharm.*, **26**, 791 (2000).
40. T. Ostberg, E. M. Lund and C. Graffner, Calcium alginate matrices for oral multiple unit administration: IV. Release characteristics in different media, *Int. J. Pharm.*, **112**, 241 (1994).
41. H. Daemi and M. Barikani, Synthesis and characterization of calcium alginate nanoparticles, sodium homopolymannuronate salt and its calcium nanoparticles, *Sci. Iran*, **19**, 2023 (2012).
42. S. R. Saptarshi, A. Duschl and A. L. Lopata, Interaction of nanoparticles with proteins: relation to bio-reactivity of the nanoparticle, *J. Nanobiotechnology*, **11**, 26 (2013).
43. Y. Cheng, S. Yu, X. Zhen, X. Wang, W. Wu and X. Jiang, Alginic acid nanoparticles prepared through counterion complexation method as a drug delivery system, *ACS Appl Mater Interfaces*, **4**, 5325 (2012).
44. P. Sundarrajan, P. Eswaran, A. Marimuthu, L. B. Subhadra and P. Kannaiyan, One pot synthesis and characterization of alginate stabilized semiconductor nanoparticles, *Bull. Korean Chem. Soc.*, **33**, 3218 (2012).
45. S. Sharma, P. Sanpui, A. Chattopadhyay and S. S. Ghosh, Fabrication of antibacterial silver nanoparticle—sodium alginate–chitosan composite films, *Rsc Advances*, **2**, 5837 (2012).
46. A. Aina, M. Gupta, Y. Boukari, A. Morris, N. Billa and S. Doughty, Monitoring model drug microencapsulation in PLGA scaffolds using X-ray powder diffraction, *Saudi Pharm J*, **24**, 227 (2016).
47. A. Verma, M. Sharma, N. Verma and J. K. Pandit, Floating alginate beads: studies on formulation factors for improved drug entrapment efficiency and in vitro release, *Farmacia*, **61**, 143 (2013).
48. R. Kotcherlakota, A. K. Barui, S. Prashar, M. Fajardo, D. Briones, A. Rodríguez-Diéguez, C. R. Patra and S. Gómez-Ruiz, Curcumin loaded mesoporous silica: an effective drug delivery system for cancer treatment, *Biomater. Sci.*, **4**, 448 (2016).
49. S. Kumar, G. Bhanjana, R. K. Verma, D. Dhingra, N. Dilbaghi and K. H. Kim, Metformin-loaded alginate nanoparticles as an effective antidiabetic agent for controlled drug release, *J Pharm Pharmacol*, **69**, 143 (2017).
50. S. Kumar, G. Bhanjana, A. Kumar, K. Taneja, N. Dilbaghi and K.-H. Kim, Synthesis and optimization of ceftriaxone-loaded solid lipid nanocarriers, *Chem. Phys. Lipids*, **200**, 126 (2016).
51. A. Manuja, S. Kumar, N. Dilbaghi, G. Bhanjana, M. Chopra, H. Kaur, R. Kumar, B. K. Manuja, S. K. Singh and S. C. Yadav, Quinapyramine sulfate-loaded sodium alginate nanoparticles show enhanced trypanocidal activity, *Nanomed.*, **9**, 1625 (2014).